land

MDPI

Article

Lagged Vegetation Responses to Diurnal Asymmetric Warming and Precipitation During the Growing Season in the Yellow River Basin: Patterns and Driving Mechanisms

Zeyu Zhang [1], Fengman Fang [1,2,*] and Zhiming Zhang [1,2]

[1] School of Geography and Tourism, Anhui Normal University, Wuhu 241003, China; zhangzeyu@ahnu.edu.cn (Z.Z.); 2022032@ahnu.edu.cn (Z.Z.)
[2] Anhui Provincial Key Laboratory of Earth Surface Processes and Response in the Yangtze-Huaihe River Basin, Wuhu 241003, China
* Correspondence: ffm1974@mail.ahnu.edu.cn

Abstract

Diurnally asymmetric warming under global climate change is reshaping terrestrial ecosystems, with important implications for vegetation productivity, biodiversity, and carbon sequestration. However, the mechanisms underlying the delayed and differentiated vegetation responses to daytime and nighttime warming, particularly under interacting precipitation regimes, remain insufficiently understood, limiting accurate assessments of ecosystem resilience under future climate scenarios. Clarifying how vegetation responds dynamically to asymmetric temperature changes and precipitation, including their lagged effects, is therefore essential. Here, we analyzed the spatiotemporal evolution of growing-season Normalized Difference Vegetation Index (NDVI) across the Yellow River Basin from 2001 to 2022 using Theil–Sen median trend estimation and the Mann–Kendall test. We further quantified the lagged responses of NDVI to daytime maximum temperature (Tmax), nighttime minimum temperature (Tmin), and precipitation, and identified their dominant controls using partial correlation analysis and an XGBoost–SHAP framework. Results show that (1) growing-season climate in the YRB experienced pronounced diurnal warming asymmetry: Tmax, Tmin, and precipitation all increased, but Tmin rose substantially faster than Tmax. (2) NDVI exhibited an overall increasing trend, with declines confined to only 2.72% of the basin, mainly in Inner Mongolia, Ningxia, and Qinghai. (3) NDVI responded to Tmax, Tmin, and precipitation with distinct lag times, averaging 43, 16, and 42 days, respectively. (4) Lag times were strongly modulated by topography, soil properties, and hydro-climatic background. Specifically, Tmax lag time shortened with increasing elevation, soil silt content, and slope, while showing a decrease-then-increase pattern with potential evapotranspiration. Tmin lag time lengthened with elevation, soil sand content, and soil pH, but shortened with higher potential evapotranspiration. Precipitation lag time increased with soil silt content and net primary productivity, decreased with soil pH, and varied nonlinearly with elevation (decrease then increase). By explicitly linking diurnal warming asymmetry to vegetation response lags and their environmental controls, this study advances process-based understanding of climate–vegetation interactions in arid and semi-arid regions. The findings provide a transferable framework for improving ecosystem vulnerability assessments and informing adaptive vegetation management and conservation strategies under ongoing asymmetric warming.

Keywords: diurnal asymmetric warming; precipitation; NDVI; driver factor

Check for updates

Received: 2 December 2025
Revised: 7 January 2026
Accepted: 8 January 2026
Published: 10 January 2026

Copyright: © 2026 by the authors. Licensee MDPI, Basel, Switzerland. This article is an open access article distributed under the terms and conditions of the Creative Commons Attribution (CC BY) license.

1. Introduction

Vegetation responses to climate change constitute a central issue in terrestrial ecosystem research, as temperature and precipitation directly regulate plant growth processes and ecosystem functioning. Remotely sensed vegetation indices, particularly the Normalized Difference Vegetation Index (NDVI), have been widely used to quantify vegetation dynamics and their responses to climate variability across different spatial and temporal scales [1–5]. The Intergovernmental Panel on Climate Change (IPCC) Global Assessment Report [6] and the Global Carbon Project [7] both highlight that NDVI is a key factor reflecting terrestrial-atmospheric feedback mechanisms and mitigating warming effects. Its dynamic changes have become a central topic in global climate change research [8]. Understanding how vegetation responds to changing climate conditions is therefore critical for assessing ecosystem stability under ongoing global warming.

Observational data indicate marked diurnal asymmetry in global warming [9–11]. Over the past half-century, the rate of nighttime temperature increase (represented by the minimum daily temperature, Tmin) has been approximately 40% faster than that of daytime temperatures (represented by the maximum daily temperature, Tmax), leading to a narrowing of the diurnal temperature range. This asymmetric warming is likely to intensify in the coming decades. Over the past half-century, the rate of nighttime temperature increase (represented by the minimum daily temperature, Tmin) has been approximately 40% faster than that of daytime temperatures (represented by the maximum daily temperature, Tmax), leading to a narrowing of the diurnal temperature range. This asymmetric warming is likely to intensify in the coming decades [12]. Diurnal asymmetric warming will have profound impacts on terrestrial vegetation systems [13,14]. During the daytime, plant growth is primarily driven by photosynthesis, which is sensitive to Tmax. In contrast, respiration occurs continuously throughout the day and night and is jointly regulated by both Tmax and Tmin. The distinct temperature responses of these two physiological processes determine the differentiated growth strategies of plants between day and night [12]. Existing studies have shown that diurnal warming affects leaf carbon allocation differently in the Tibetan Plateau region [15]. In the western Songnen Plain, summer daytime temperature (Tmax) increases suppress plant net primary productivity in wetlands, whereas nighttime temperature (Tmin) increases promote it [16]. Furthermore, the same vegetation type exhibits a clear asymmetric lag response to daytime and nighttime temperature changes [17]. Climate warming has a profound impact on the precipitation sensitivity of different regions [18]. The vulnerability of vegetation to precipitation changes is increasing [19]. Research has shown that vegetation in the Inner Mongolian grasslands is more sensitive to precipitation than in deserts and forests [20]. The impact of precipitation on vegetation growth in the karst regions of southern China is greater than that of temperature, with vegetation growth in southern regions being more sensitive to precipitation depending on geological conditions [21]. In summary, climate change is increasingly affecting vegetation, with noticeable regional differences in the impact of diurnal warming and precipitation. However, most studies neglect to investigate the reasons for differences in lag times within the study areas. The temporal lag characteristics and their controlling mechanisms under combined diurnal asymmetric warming and precipitation variability remain insufficiently explored.

As one of the key regions affected by global warming [22,23], the Yellow River Basin has experienced notable impacts of climate change on its vegetation [24,25]. Systematically investigating the response processes and mechanisms of vegetation to climate change in this region holds both theoretical importance and practical urgency. This study aims to systematically reveal the time-lag response of vegetation in the Yellow River Basin to diurnal asymmetric warming and precipitation variations. The specific objectives are as follows: (1) To characterize the spatial pattern and temporal evolution of vegetation

cover (NDVI) during the growing season (April 1–October 31) from 2001 to 2022. (2) To calculate the lag time of NDVI responses to diurnal asymmetric warming and precipitation variations using partial correlation analysis. (3) To elucidate the driving mechanisms of multiple influencing factors on the lag time by integrating the eXtreme Gradient Boosting (XGBoost) algorithm and the SHapley Additive exPlanations (SHAP) method. The specific process of this study is shown in Figure 1.

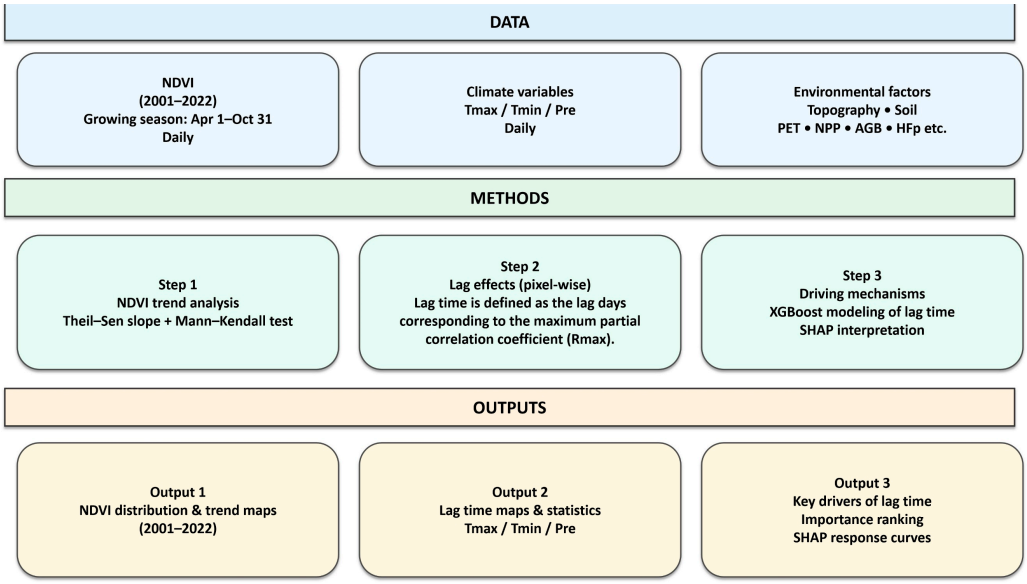

Figure 1. Research process flowchart.

2. Materials and Methods

2.1. Study Area

The Yellow River Basin (32° N–42° N, 96° E–119° E) (Figure 2) spans across nine provinces and autonomous regions in China, covering a total area of approximately 7.95×10^5 km^2. The terrain of the basin generally decreases from west to east, forming a three-tiered steppe with an elevation difference of 4480 m. This region is characterized by three climate zones: arid, semi-arid, and semi-humid. The daily temperature variation within the basin is relatively large, with daily temperature differences ranging from 13 °C to 16.5 °C throughout the year. Precipitation in the basin is unevenly distributed, ranging from 200 to 1000 mm. The ecological environment is diverse, with grasslands, shrublands, mixed forests, and deciduous forests, among others. The basin serves as an ecological corridor linking the Tibetan Plateau, Loess Plateau, and North China Plain. It plays a crucial role in both China's economic development and its ecological security. Investigating the lag effect mechanisms of vegetation and revealing the specific impacts of climate change on regional ecosystems can provide valuable scientific support for the ecological protection and restoration of the basin, helping address the ecological threats posed by climate change and promoting regional sustainable development.

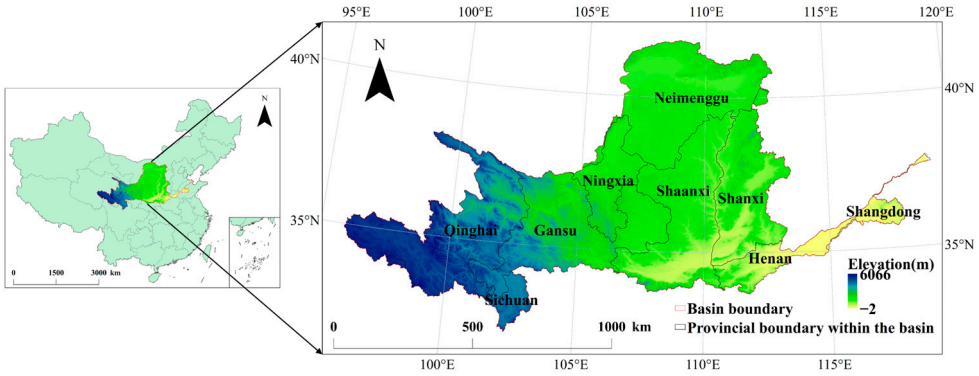

Figure 2. Location of the research area. Darker colors indicate higher elevations. The map data was obtained from the Ministry of Natural Resources of the People's Republic of China [Drawing review No. GS (2024) 0650].

2.2. Data Sources and Processing

2.2.1. NDVI Data

The NDVI data utilized in this study were obtained from the Shaanxi Key Laboratory of Qinling Ecological Intelligent Monitoring and Protection, School of Ecology and Environment, Northwestern Polytechnical University, with a spatial resolution of 0.05° × 0.05° [26].

2.2.2. Temperature and Precipitation Data

The Tmax, Tmin, and precipitation data were obtained from a multisource integrated high-resolution multi-variable meteorological dataset for China. The dataset has a spatial resolution of 0.01° × 0.01° [27].

2.2.3. Other Data

To analyze the factors contributing to the differences in lag time, we incorporated data on topography, soil, and other related variables. The data used and its sources are shown in Table 1.

Table 1. Explanatory variable data.

Data	Source
Digital elevation model data	https://www.gscloud.cn (accessed on 3 September 2025)
Potential evapotranspiration data	https://data.tpdc.ac.cn (accessed on 10 September 2025)
Soil property data	https://www.earth-system-science-data.net (accessed on 11 September 2025)
Net primary productivity data	https://lpdaac.usgs.gov (accessed on 11 September 2025)
The human footprint dataset	https://www.x-mol.com/groups/li_xuecao (accessed on 12 September 2025)
The biomass dataset	https://code.earthengine.google.com (accessed on 12 September 2025)

All datasets span the period from 2001 to 2022 and were harmonized to a spatial resolution of 0.05° × 0.05°. Specifically, for continuous meteorological variables originally at finer spatial resolutions, values were upscaled by grid-cell aggregation (averaging) to the target 0.05° grid. For influencing factors involving multi-year data, multi-year means were calculated.

2.3. Methods

2.3.1. Trend Analysis

The Theil–Sen median method is a robust nonparametric statistical approach for trend estimation [28]. It is insensitive to measurement errors and outliers, making it widely

utilized in long-term time series trend analyses. The Mann–Kendall test treats a time series as n independent random samples from an identical distribution. Its advantages lie in not requiring the data to follow a specific distribution and in being less affected by extreme values.

$$\beta = median\frac{x_j - x_i}{j - i}, 1 < i < j < n \quad (1)$$

In the equation, n represents the number of study years, x_i denotes the NDVI value in the i-th year, and β is the trend magnitude. A negative β indicates a decreasing trend, whereas a positive β indicates an increasing trend.

2.3.2. De-Trended

Prior to performing the lag correlation analysis, the time series were de-trended to minimize the effects of seasonal cycles and long-term trends on the estimated relationships. Time series data typically contain both seasonal periodicity and long-term trends, which need to be removed from the original series. First, a simple linear regression model was applied to extract the linear trend component, expressed as follows:

$$y_t^T = a_1 + a_2 t \quad (2)$$

where $\hat{y}_t^T$ represents the predicted trend component, t denotes time, and a_1 and a_2 are the intercept and slope of the regression, respectively, estimated using the least squares method.

The seasonal component $\hat{y}_t^S$ was derived from the multi-year daily mean values. By subtracting both the trend component $\hat{y}_t^T$ and the seasonal component $\hat{y}_t^S$ from the original time series y_t, a stationary residual series $\hat{y}_t^R$ was obtained:

$$y_t^{\mathrm{R}} = y_t - y_t^{\mathrm{T}} - y_t^{\mathrm{S}} \quad (3)$$

2.3.3. Lag Effects

In this study, a partial correlation analysis [12,17] was employed to examine the independent relationship between NDVI and a single meteorological variable (Tmax, Tmin, or precipitation) while controlling for the other two potential confounding variables.

$$r_{XY|Z_1Z_2} = \frac{r_{XY} - r_{XZ_1} \cdot r_{YZ_1}}{\sqrt{\left(1 - r_{XZ_1}^2\right)\left(1 - r_{Z_1Z_2}^2\right)}} \quad (4)$$

where $r_{XY|Z_1Z_2}$ represents the partial correlation coefficient between variables X and Y after controlling for variables Z_1 and Z_2; r_{XZ}, r_{XZ_1} and r_{XZ_2} denote the Pearson correlation coefficients between the corresponding variable pairs.

The maximum partial correlation coefficient (R_{max}) was selected, and the corresponding lag days were regarded as the time scale of the lag effect for each pixel.

$$R_{max} = corr(NDVI, Y),\ 1 \leq i \leq 90 \quad (5)$$

where $NDVI$ represents the daily NDVI time series from 2001 to 2022 during the growing season, Y denotes the time series of the meteorological variable lagged by i days, and R_{max} is the maximum lag correlation coefficient.

2.3.4. XGBoost

To explore the relationship between the driving factors and lag time, this study employed the XGBoost machine learning algorithm to analyze the results of the lag time prediction model. Fourteen vegetation growth-related variables were incorporated into

the analysis [29], including elevation (ELE), slope (SLO), aspect (ASP), soil total nitrogen (TN), soil total phosphorus (TP), soil organic carbon (OC), soil sand content (Sand), soil silt content (Silt), soil clay content (Clay), potential evapotranspiration (Pet), net primary production (NPP), aboveground biomass (AGB), and human footprint (HFp). The objective function of XGBoost can be expressed as follows:

$$L(\theta) = \sum_{i=1}^{n} l(y_i, \hat{y}_i) + \sum_{k=1}^{K} \Omega(f_k) \tag{6}$$

Here, $L(\theta)$ represents the expression in linear space; i denotes the ith sample; k refers to the kth tree; y_i is the true value of the ith sample; $\hat{y}_i$ represents the predicted value of the ith sample; $l(y_i, \hat{y}_i)$ is the loss function that measures the prediction error for each sample; and $\Omega(f_k)$ is the regularization term utilized to control model complexity.

To optimize the objective function and minimize the loss, XGBoost applies a second-order Taylor expansion to the objective function. After discarding the constant terms unrelated to the model, the simplified objective function can be expressed as follows:

$$L(t) \ = \sum_{i=1}^{n} \left[g_i \, f_t(x_i) + \frac{1}{2} h_i \, f_t^{\,2}(x_i) \right] + \Omega(f_t) \tag{7}$$

In the equation, g_i denotes the first-order derivative of the loss function with respect to the data, and hi represents the second-order derivative of the loss function with respect to the data.

2.3.5. SHAP Algorithm

SHAP (SHapley Additive exPlanations) is a method for model interpretability. It quantifies the contribution of each input feature to the prediction results of a machine learning model. It attributes the output value to individual features through their corresponding Shapley values, thereby assessing the influence of each driving factor on the final prediction outcome [29].

$$\varphi_i = \sum_{S \subseteq N \setminus \{i\}} \frac{|S|!(M - |S| - 1)!}{M!} \left[f_{S \cup \{i\}}(x) - f_S(x) \right] \tag{8}$$

In the equation, φ_i denotes the Shapley value of feature i. M represents the total number of features. N is the complete set of all features. S indicates a subset of N that excludes feature i, and $f_S(x)$ is a function representing the model's predicted value based on the feature combination in subset S.

3. Results

3.1. Changes in Tmax, Tmin, and Precipitation During the Growing Season

Tmax, Tmin, and precipitation all exhibit a generally fluctuating upward trend (Figure 3). Notably, the warming rate of Tmax (0.036 °C/10a) is markedly lower than that of Tmin (0.38 °C/10a), indicating a pronounced asymmetry in the daytime and nighttime warming in the Yellow River Basin (Figure 3a). Tmax reached its minimum value of 19.75 °C in 2003 and peaked at 21.21 °C in 2013, while Tmin recorded its lowest value of 7.98 °C in 2004 and its highest value of 9.33 °C in 2022. The annual average precipitation in the growing season showed a growth rate of 2.26 mm/a (Figure 3b), with the fastest increase occurring between 2008 and 2013, at a rate of 11.46 mm/a. The minimum annual precipitation was recorded in 2015 (361.63 mm), while the maximum occurred in 2003 (517.23 mm).

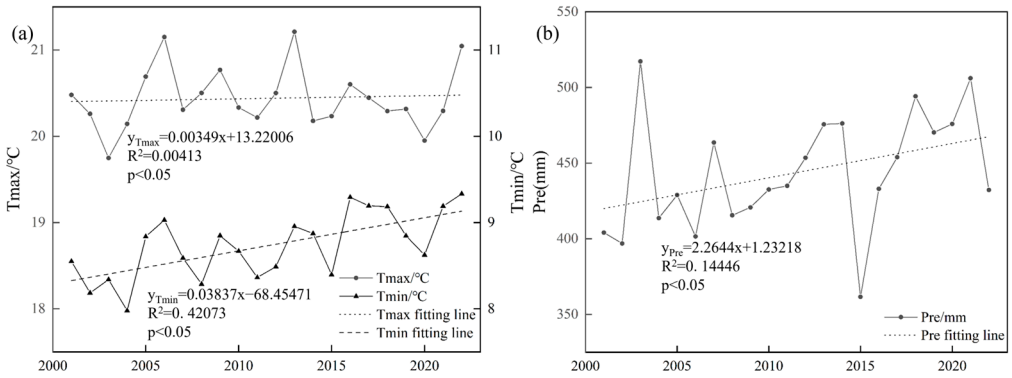

Figure 3. Annual variation trends of Tmax, Tmin and precipitation in the growing season. (**a**) Change in average diurnal–nocturnal temperatures from 2001 to 2022. (**b**) Change in precipitation from 2001 to 2022.

3.2. Spatial Distribution and Trend of NDVI During the Growing Season

The average NDVI value during the growing season from 2001 to 2022 was 0.36 (Figure 4a). High NDVI values were mainly concentrated in the southern regions of the Yellow River Basin, such as Shaanxi and Henan provinces, while low-value areas were primarily located in the northwestern provinces, including Gansu, Ningxia, and Inner Mongolia. Trend analysis and statistical tests were applied to examine the spatial distribution of NDVI changes (Figure 4b). The results revealed that, from 2001 to 2022, most areas within the study region experienced a significant increase in NDVI. The area with a significant increase covers approximately 7.36×10^5 square kilometers, accounting for about 92.67% of the total area of the study region. 3.00% of the area showed no significant increase, 1.6% remained stable, 0.97% showed no significant decrease, and 1.75% exhibited a significant decrease. The degraded areas are relatively minor and are mainly located in Inner Mongolia, Ningxia Hui Autonomous Region, and Qinghai Province.

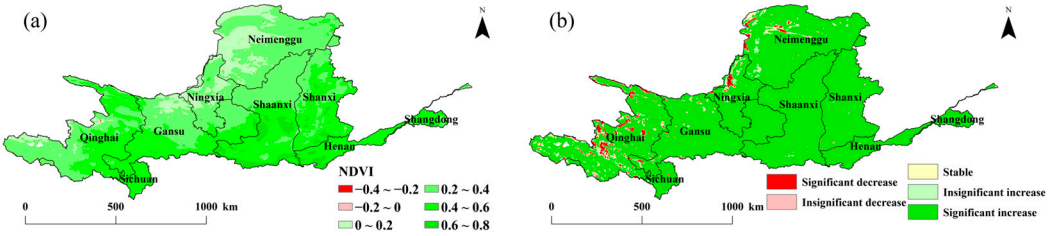

Figure 4. Trends in NDVI changes during the growing season: (**a**) Spatial distribution of the multi-year mean NDVI. (**b**) Multi-year NDVI change trend.

3.3. Lag Effects of Tmax, Tmin, and Precipitation on NDVI During the Growing Season

3.3.1. Lag Effects of Tmax and Tmin on NDVI

In the Yellow River Basin, 99.98% of the area showed a positive correlation between NDVI and Tmax (Figure 5), with only 0.02% of the area showing a negative correlation. Of the positive correlations, 99.15% passed the significance test with $p \leq 0.05$. The average partial correlation coefficient is 0.64, with higher coefficients primarily concentrated in the southern regions of the Yellow River Basin, including Shaanxi and Gansu provinces. Overall, the average lag time of Tmax on vegetation growth is 43 days, with longer lag times mainly occurring in the downstream and midstream areas of the Yellow River Basin. Regarding Tmin, 99.29% of the area in the Yellow River Basin showed a positive correlation between NDVI and Tmin (Figure 6), with only 0.92% exhibiting a negative correlation. Among the positive correlations, 99.15% passed the significance test with $p \leq 0.05$. Areas with higher partial correlation coefficients are mainly located in the central regions of the

Yellow River Basin, including Gansu, Ningxia Hui Autonomous Region, southern Inner Mongolia, Shaanxi, Shanxi, and the downstream Shandong Province, with an average partial correlation coefficient of 0.74. The overall average lag time is 16 days, with longer lags concentrated in the upstream areas of the Yellow River Basin. This suggests that both Tmax and Tmin have a significant promoting effect on vegetation growth in the Yellow River Basin, with vegetation responding more quickly to Tmin.

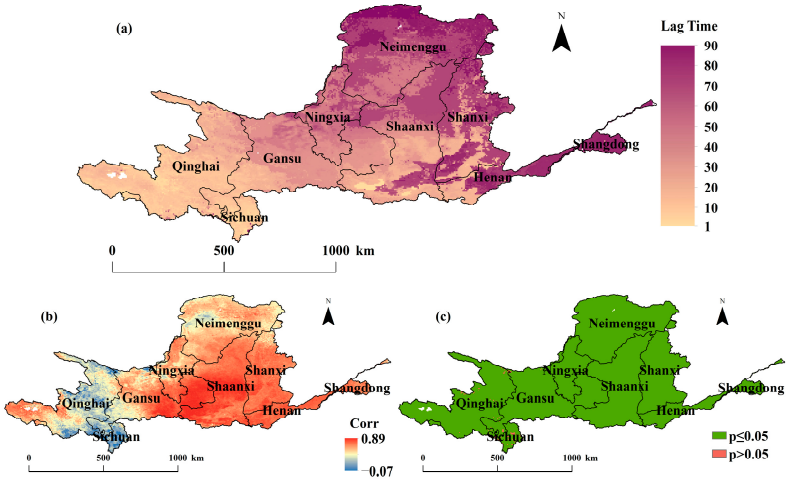

Figure 5. Lag effect of NDVI on Tmax during the growing season. (**a**) Lag time. (**b**) Maximum partial correlation coefficient. (**c**) Statistical significance.

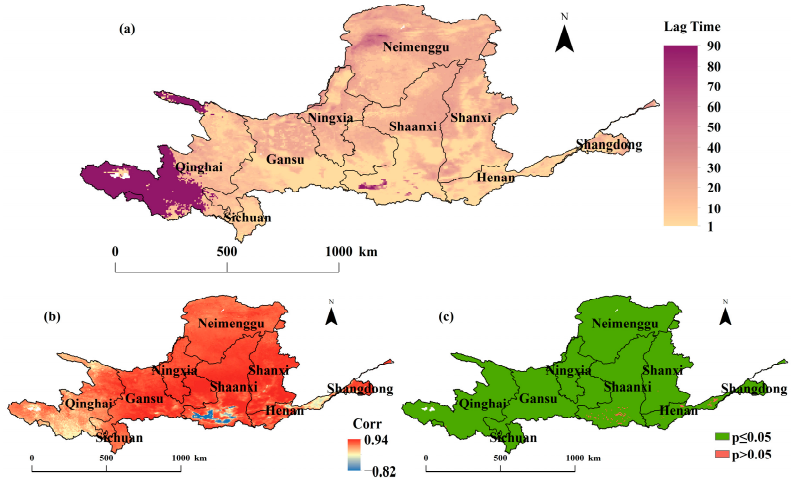

Figure 6. Lag effect of NDVI on Tmin during the growing season. (**a**) Lag time. (**b**) Maximum partial correlation coefficient. (**c**) Statistical significance.

3.3.2. Lag Effects of Precipitation on NDVI During the Growing Season

As for precipitation, 98.76% of the area in the Yellow River Basin showed a positive correlation between NDVI and precipitation (Figure 7), with only 1.24% exhibiting a negative correlation. Among the positive correlations, 70.37% passed the significance test with $p \leq 0.05$, and 22.21% passed the more stringent test with $p \leq 0.05$. Areas with higher partial correlation coefficients are primarily located in the southwestern regions of the Yellow River Basin, such as Sichuan and Qinghai provinces, with an average partial correlation coefficient of 0.19. The overall average lag time was 42 days, with a spatial pattern where the lag time was longer in the southern part of the basin compared to the northern areas.

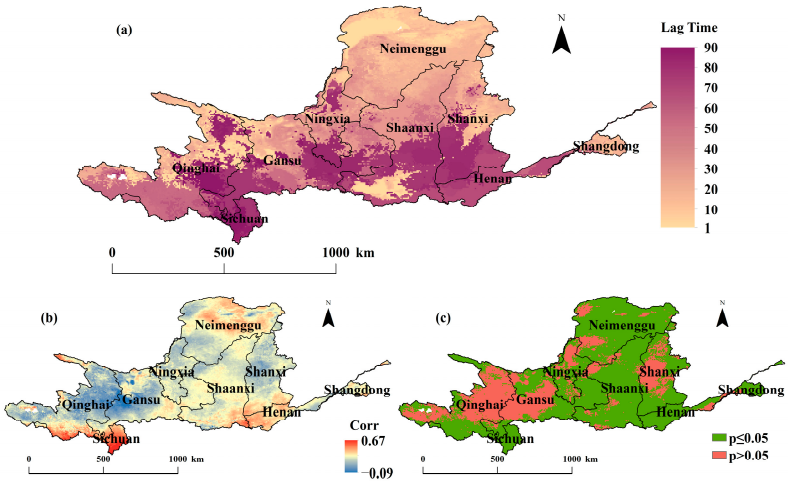

Figure 7. Lag effect of NDVI on precipitation during the growing season. (**a**) Lag time. (**b**) Maximum partial correlation coefficient. (**c**) Statistical significance.

In summary, the relationship between vegetation growth and temperature and precipitation in the Yellow River Basin exhibits significant spatial and temporal differences. Tmax has a stronger promoting effect on vegetation growth in the southern part of the basin, while vegetation growth is more sensitive to Tmin, with a broader area of response and shorter lag times. Precipitation generally promotes NDVI in most regions, although its impact on vegetation growth is less intense.

3.4. Factors Contributing to Differences in Lag Effect Patterns

In the simulation of lag times for the effects of Tmax, Tmin, and precipitation on NDVI, the models achieved R^2 values of 0.93 and 0.90 for the test and training sets, 0.91 and 0.89, and 0.95 and 0.89, respectively. This suggested that the models have favorable applicability to the entire dataset and strong explanatory power. In this study, the four most important influencing factors were selected to analyze the causes of lag time differences. Elevation, clay content, potential evapotranspiration, and slope are the key factors causing differences in the lag time of Tmax's effect on NDVI (Figure 8). Elevation, sand content, potential evapotranspiration, and soil pH are the main factors responsible for the lag time differences in Tmin's effect on NDVI (Figure 9). Clay content, elevation, soil pH, and NPP are the critical factors leading to lag time differences in the impact of precipitation on NDVI (Figure 10).

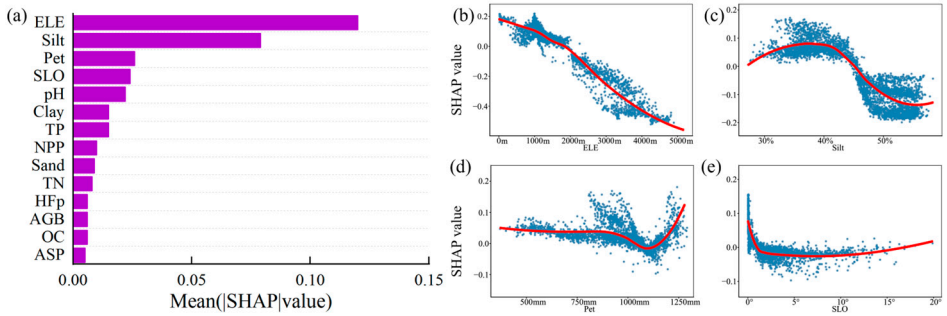

Figure 8. Factors affecting the lag duration of NDVI's response to Tmax, (**a**) ranking of the relative importance of factors, (**b**–**e**) are the four most important explanatory variables, (**b**) elevation, (**c**) silt content, (**d**) potential evapotranspiration, (**e**) slope.

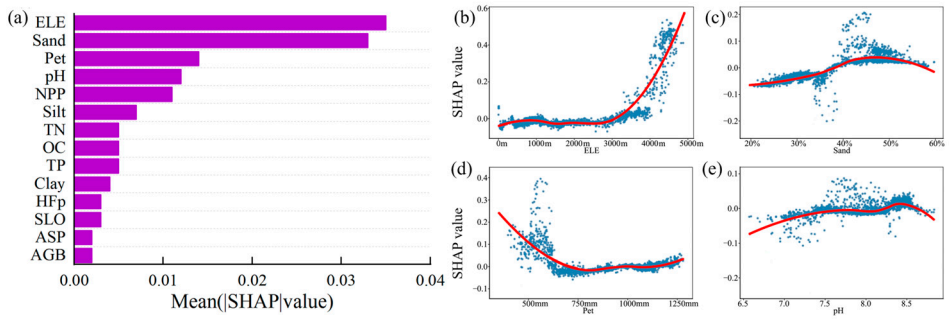

Figure 9. Factors affecting the lag duration of NDVI's response to Tmin, (**a**) ranking of the relative importance of factors, (**b**–**e**) are the four most important explanatory variables, (**b**) elevation, (**c**) sand content, (**d**) potential evapotranspiration, (**e**) soil pH.

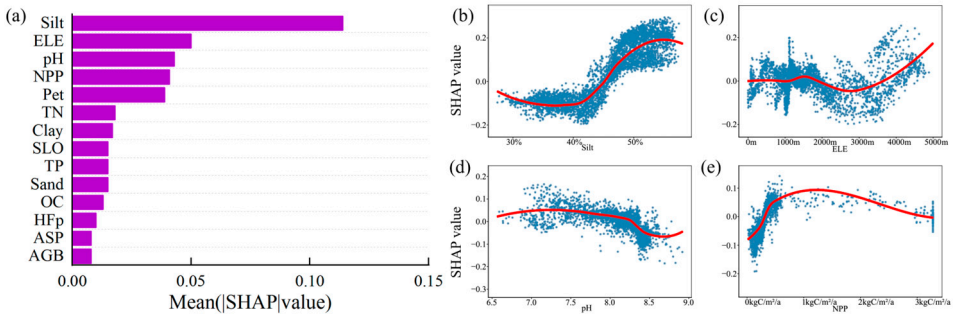

Figure 10. Factors affecting the duration of NDVI's lagged response to precipitation, (**a**) ranking of the relative importance of factors, (**b**–**e**) are the four most important explanatory variables, (**b**) silt content, (**c**) elevation, (**d**) soil pH, (**e**) Net Primary Productivity.

4. Discussion

4.1. Spatiotemporal Evolution of NDVI During the Growing Season

From 2001 to 2022, the vegetation in the Yellow River Basin exhibited an overall upward trend, which is generally consistent with previous studies [30,31]. This suggested that the natural forest protection project, the Three-North Shelterbelt Forest Program, and the Grain for Green Program implemented in China have had considerable effects in improving the ecological environment that supports vegetation growth and development [32].

From a temporal perspective, between 1979 and 2018, the afforestation area of the Three-North Shelterbelt Program reached 30 million hectares. The forest coverage rate in northern China increased from 5.05% in 1979 to 13.57% in 2018 [33], with young forests being predominant. The dominance of young forests indicated that the forest ecosystem is generally in a vigorous growth phase [34], and NDVI values will continue to rise.

Looking at the spatial distribution, most areas in the Yellow River Basin show an upward trend in growing season NDVI. Additionally, in the southern part of the study area, where water and heat conditions are more favorable, NDVI values are higher than those in the northwest [35]. In some areas of Inner Mongolia, Ningxia Hui Autonomous Region, and Qinghai Province, however, NDVI has significantly decreased. These areas have relatively fragile ecosystems, and excessive human activities such as deforestation and grazing have damaged the natural ecosystems, exacerbating environmental issues [36].

4.2. Promoting Effects of Tmax, Tmin, and Precipitation on NDVI in the Yellow River Basin During the Growing Season

The results of the impact of diurnal asymmetric warming and precipitation on vegetation are generally consistent with previous studies [37,38]. During the growing season in the Yellow River Basin, Tmax predominantly promotes vegetation growth. During the

day, vegetation absorbs sunlight through photosynthesis. Daytime warming facilitates an increase in photosynthetic enzyme activity, promotes the opening of stomata in plant leaves, and enhances vegetation productivity [11]. This also increases the probability of CO_2 entering the leaves for photosynthesis, thereby promoting vegetation growth, as reflected in the rise in NDVI [39].

The lag time of NDVI to Tmin is shorter than that to Tmax, and vegetation's positive response to Tmin is more immediate [40]. Nighttime temperature primarily affects plant respiration, especially during the growing season, where vegetation's response to nighttime temperature is more direct. Although nighttime respiration consumes some organic matter, reducing net accumulation, the intensification of autotrophic respiration at night can generate a compensatory effect, thus enhancing plant productivity and promoting more carbon accumulation [41]. Elevated nighttime temperatures help plants recover and maintain higher biomass, thereby improving the efficiency of daytime photosynthesis and promoting plant growth. Specifically, during the growing season, warm nights facilitate plants maintaining higher biomass, and an increase in Tmin can extend the growing season. Previous studies have shown that the promoting effect of elevated nighttime temperatures on plants is more pronounced [42]. Nighttime warming can also advance the flowering and fruiting times of some species [43].

The positive influence of growing-season precipitation on NDVI in the Yellow River Basin is weaker than that of temperature. The vegetation's response to precipitation is generally lower in terms of both partial correlation coefficients and significance when compared to temperature. This is related to the vegetation's water-use mechanisms [44,45]. Precipitation can rapidly alter soil moisture conditions, improve the growth environment, and promote vegetation growth. However, in the arid and semi-arid regions of the Yellow River Basin, vegetation showed lower sensitivity to precipitation [46]. Vegetation reduces resource consumption by maintaining leaf stability, forming water conservation strategies that adapt to the arid environment [47].

4.3. Lag Time Differences Analysis

4.3.1. Analysis of the Driving Factors of Tmax Lag Time Differences

The lag time of NDVI's response to Tmax decreases with the increase in elevation, soil silt content, and slope, and shows a trend of first decreasing and then increasing with the rise in potential evapotranspiration. In high-altitude areas of the Yellow River Basin, lower temperatures cause Tmax to influence vegetation growth more rapidly [48]. Vegetation can respond quickly to changes in Tmax [49], resulting in a shorter lag time in the Tmax–NDVI relationship. At the same time, elevation is closely linked to temperature through the lapse-rate effect and thus partly reflects the background thermal gradient. In this context, elevation acts not only as a topographic factor but also as an integrated proxy for temperature-related and micro-climatic conditions, such as air pressure and radiation regimes, which jointly modulate vegetation sensitivity to Tmax variability. Higher silt content in the soil helps absorb and retain more moisture. This enables vegetation in the arid and semi-arid regions of the Yellow River Basin to maintain a better water status during the day when temperatures are high, preventing water shortages due to excessive evaporation [50]. As a result, the effect of Tmax on NDVI is accelerated, shortening the lag time. In the Yellow River Basin, areas with high potential evapotranspiration are mostly distributed in the downstream regions of the study area. Water supply is also more abundant downstream [51], allowing vegetation to respond more quickly to temperature changes, thus shortening the lag time [52]. However, in the northern slopes of the Qinling Mountains along the southern boundary of the Yellow River Basin, where potential evapotranspiration exceeds approximately 1100 mm, water ceases to be the primary limiting

factor for vegetation growth during the day. Vegetation growth is further influenced by light and temperature. In such areas, an increase in Tmax may be accompanied by excessive transpiration and stomatal closure, which increases the lag time of NDVI's response to Tmax [53,54]. In regions with steep slopes in the Yellow River Basin, soil and nutrient loss is severe [55]. Moreover, the increase in slope leads to faster heat dissipation [56]. Therefore, plants in these steeper areas of the study region are likely to respond more quickly to daytime temperature changes, resulting in a shorter lag time. In areas with gentler slopes, the water and heat conditions are more stable, and the vegetation's response to Tmax changes tends to have a longer lag time.

4.3.2. Analysis of the Driving Factors of Tmin Lag Time Differences

The lag time of Tmin's effect on NDVI increases with elevation, soil sand content, and soil pH, but decreases with the rise in potential evapotranspiration. In the study area, high-altitude regions exhibit a longer lag effect of Tmin. This is likely due to the weaker heat retention of the atmosphere at high altitudes [57], leading to greater diurnal temperature fluctuations. As a result, plant metabolic activities are suppressed by the lower night-time temperatures [56], thereby extending the impact of Tmin on vegetation growth. In regions of the Yellow River Basin with higher soil sand content, the soil's heat retention and water-holding capacity are poor [58,59]. Consequently, vegetation growth is more affected by the drop in temperature at night [60], which leads to a longer lag time. In areas where potential evapotranspiration is less than approximately 770 mm, the water and heat conditions are poorer, limiting the evapotranspiration process. With tighter water supply and lower soil moisture, vegetation becomes more sensitive to Tmin variations [61]. In regions where potential evapotranspiration exceeds 770 mm, water supply is more abundant. This stabilizes vegetation physiological activity and lengthens the lag time to Tmin temperature changes [62]. Saline-alkali soils are distributed across the upstream, midstream, and downstream regions of the Yellow River Basin [63]. In areas with higher soil alkalinity, the soil's water retention and aeration capacities are poor [64], making it more difficult for plants to absorb water. As a result, their response to temperature changes is slower. During nighttime temperature fluctuations, plants reduce water evaporation. They do this by suppressing respiration and transpiration [24]. This further extends the effect of Tmin on NDVI.

4.3.3. Analysis of the Driving Factors of Precipitation Lag Time Differences

Regarding precipitation, the lag time increases with the increase in soil silt content and NPP, decreases with soil pH, and shows a trend of first decreasing and then increasing with elevation. Soils with higher silt content tend to provide greater plant-available water, thereby sustaining moisture availability for vegetation for a longer period after precipitation events [48]. In contrast, although clay-rich soils often have higher total water retention, a larger fraction of water is tightly bound and less available to plants. Therefore, the prolonged post-precipitation water supply under silt-rich conditions can extend vegetation responses, resulting in a longer lag time of NDVI to precipitation. This extends the water supply time for vegetation after precipitation, resulting in a longer lag time for NDVI's response to precipitation. In the low-altitude areas of the Yellow River Basin, precipitation is relatively stable [65,66]. The changes in NDVI after precipitation are relatively synchronous. As elevation increases, the lag time showed a trend of first decreasing and then increasing. This may be related to the maximum precipitation altitude zone, where precipitation is more concentrated in this zone. This area is primarily located in the southern part of the upper Yellow River Basin, where the vegetation's lag time to precipitation shortens. Beyond this elevation zone, precipitation decreases with increasing mountain altitude, resulting in

slower water supply and a longer lag time. Neutral soil pH ($6.5 \leq pH < 7.5$) [67] typically provides a more balanced growing environment for vegetation, allowing plants to better absorb water and nutrients. The effect of precipitation on vegetation is moderate, and the lag time does not show considerable changes with increasing pH. In alkaline soil in the Yellow River Basin, water retention is poor [64]. Precipitation reduces soil salinity [68]. This allows vegetation to respond more quickly to precipitation, reducing the lag time. In regions of the basin with lower NPP, vegetation has lower photosynthetic efficiency [69]. As NPP increases, plant growth and water demand rise, causing NDVI changes after precipitation to take longer to manifest. When NPP is high, the effect of precipitation on NDVI becomes stable [70], with no marked trend in lag time changes.

4.4. Limitations

This study revealed the lag times of NDVI to diurnal asymmetrical warming and precipitation during the growing season in the Yellow River Basin. It also analyzed the influence of various environmental factors, such as topography and soil texture, on vegetation responses. However, the study has some limitations. Due to data limitations, this study did not explicitly distinguish between natural vegetation and croplands. Given that irrigation and other management practices can substantially alter water availability and thereby modulate vegetation's lag responses to climatic drivers, separating natural and agricultural systems should be a priority in future research [8,33]. Lastly, this study's limitations are mainly due to the low spatial resolution (0.05°) of the NDVI data, which may fail to capture fine-scale vegetation changes [71]. While key factors such as elevation, soil type, and precipitation were considered, other important variables, like land-use changes, were excluded due to data constraints [72]. Additionally, we analyzed lag responses by aggregating the entire growing season. Vegetation responses may differ between spring green-up and autumn senescence, potentially leading to phase-dependent lag patterns. Future work could examine these sub-periods separately to better capture such seasonal heterogeneity.

5. Conclusions

This study examined the spatiotemporal variation in NDVI in the Yellow River Basin from 2001 to 2022, assessed the lag effects of diurnal temperature and precipitation on NDVI, and explored the main factors influencing the lag time. The specific conclusions are as follows:

1. From 2001 to 2022, NDVI in the Yellow River Basin exhibited a spatial distribution characterized by higher values in the south and lower values in the northwest, with an overall improving trend;
2. In the Yellow River Basin, due to the influences of terrain, climate, and soil, there are differences in the lag response times of NDVI to Tmax, Tmin, and precipitation. In the eastern and northern regions of the basin, the lag response time of NDVI to Tmax is longer, while in the western region, the lag response time to Tmin is longer, and in the southern region, the lag response time to precipitation is longer. Specifically, the average lag time for NDVI in response to Tmax is 43 days, to Tmin is 16 days, and to precipitation is 42 days;
3. Elevation, soil silt content, potential evapotranspiration, and slope are important factors influencing the lag time of NDVI's response to Tmax. The lag time shortens with increases in elevation, soil silt content, and slope, and it first decreases and then increases as potential evapotranspiration rises. Key drivers influencing the lag time of NDVI to Tmin include elevation, soil sand content, potential evapotranspiration, and soil pH. The lag time lengthens with increases in elevation, soil sand content, and soil pH, but decreases as potential evapotranspiration increases. Regarding precipitation,

soil silt content, elevation, soil pH, and NPP notably impact the lag time. The lag time lengthens with increasing soil silt content and NPP but decreases with higher soil pH. Additionally, the lag time shows a trend of first decreasing and then increasing with the rise in elevation.

In summary, this study makes an important and novel contribution to understanding the lag responses of vegetation to asymmetric warming, with clear implications for ecological and climate adaptation policy based on its findings.

Author Contributions: Conceptualization, Z.Z. (Zeyu Zhang) and F.F.; Methodology, Z.Z. (Zeyu Zhang); Software, Z.Z. (Zeyu Zhang); Validation, Z.Z. (Zeyu Zhang); Investigation, F.F.; Writing—original draft, Z.Z. (Zeyu Zhang); Writing—review & editing, F.F. and Z.Z. (Zhiming Zhang); Visualization, Z.Z. (Zeyu Zhang); Supervision, F.F.; Project administration, F.F. and Z.Z. (Zhiming Zhang); Funding acquisition, F.F. and Z.Z. (Zhiming Zhang). All authors have read and agreed to the published version of the manuscript.

Funding: This research was funded by the Science & Technology Fundamental Resources Investigation Program (grant number 2023FY100101) and the National Natural Science Foundation of China (grant number 42471088).

Data Availability Statement: The original contributions presented in this study are included in the article. Further inquiries can be directed to the corresponding author.

Conflicts of Interest: The authors declare no conflicts of interest.

References

1. Piao, S.; Wang, X.; Park, T.; Chen, C.; Lian, X.; He, Y.; Bjerke, J.W.; Chen, A.; Ciais, P.; Tømmervik, H.; et al. Characteristics, drivers and feedbacks of global greening. *Nat. Rev. Earth Environ.* **2020**, *1*, 14–27. [CrossRef]
2. Sha, Z.; Bai, Y.; Li, R.; Lan, H.; Zhang, X.; Li, J.; Liu, X.; Chang, S.; Xie, Y. The global carbon sink potential of terrestrial vegetation can be increased substantially by optimal land management. *Commun. Earth Environ.* **2022**, *3*, 8. [CrossRef]
3. Yin, C.; Zhao, W.; Ye, J.; Muroki, M.; Pereira, P. Ecosystem carbon sequestration service supports the Sustainable Development Goals progress. *J. Environ. Manag.* **2023**, *330*, 117155. [CrossRef]
4. Cui, L.; Wang, Z.; Deng, L.; Qu, S. Vegetation dynamics and their relations with climate change at seasonal scales in the Yangtze River Basin, China. *Appl. Ecol. Environ. Res.* **2020**, *18*, 3543–3556. [CrossRef]
5. Han, J.; Huang, Y.; Zhang, H.; Wu, X. Characterization of elevation and land cover dependent trends of NDVI variations in the Hexi region, northwest China. *J. Environ. Manag.* **2019**, *232*, 1037–1048. [CrossRef] [PubMed]
6. IPCC. *Climate Change 2021: The Physical Science Basis*; Contribution of Working Group I to the Sixth Assessment Report of the Intergovernmental Panel on Climate Change; Cambridge University Press: Cambridge, UK; New York, NY, USA, 2021; p. 2391. [CrossRef]
7. Friedlingstein, P.; Jones, M.W.; O'Sullivan, M.; Andrew, R.M.; Bakker, D.C.E.; Hauck, J.; Le Quéré, C.; Peters, G.P.; Peters, W.; Pongratz, J.; et al. Global Carbon Budget 2021. *Earth Syst. Sci. Data* **2022**, *14*, 1917–2005. [CrossRef]
8. Li, X.; Li, P.; Gao, M.; Mu, D.; Han, D. Impacts of human activities on vegetation dynamics amid climate change: A case study of the Hanjiang River Basin (China). *J. Environ. Manag.* **2025**, *391*, 126581. [CrossRef]
9. Zhong, Z.; Chen, H.; Dai, A.; Zhou, T.; He, B.; Su, B. Sub-diurnal asymmetric warming has amplified atmospheric dryness since the 1980s. *Nat. Commun.* **2025**, *16*, 8247. [CrossRef] [PubMed]
10. Zhong, Z.; He, B.; Chen, H.; Chen, D.; Zhou, T.; Dong, W.; Xiao, C.; Xie, S.; Song, X.; Guo, L.; et al. Reversed asymmetric warming of sub-diurnal temperature over land during recent decades. *Nat. Commun.* **2023**, *14*, 7189. [CrossRef] [PubMed]
11. Peng, S.; Piao, S.; Ciais, P.; Myneni, R.B.; Chen, A.; Chevallier, F.; Dolman, A.J.; Janssens, I.A.; Peñuelas, J.; Zhang, G.; et al. Asymmetric effects of daytime and night-time warming on northern hemisphere vegetation. *Nature* **2013**, *501*, 88–94. [CrossRef]
12. Xu, B.; Li, J.; Pei, X.; Yang, H. Decoupling the response of vegetation dynamics to asymmetric warming over the Qinghai-Tibet plateau from 2001 to 2020. *J. Environ. Manag.* **2023**, *347*, 119131. [CrossRef]
13. Liu, G.; Guo, Y.; Xia, H.; Liu, X.; Song, H.; Yang, J.; Zhang, Y. Increase asymmetric warming rates between daytime and nighttime temperatures over global land during recent decades. *Geophys. Res. Lett.* **2024**, *51*, e2024GL112832. [CrossRef]
14. Liu, Y.; Wu, C.; Wang, X.; Zhang, Y. Contrasting responses of peak vegetation growth to asymmetric warming: Evidences from FLUXNET and satellite observations. *Glob. Change Biol.* **2023**, *29*, 2363–2379. [CrossRef]

15. Wu, L.; Shen, X.; Lu, X.; Jiang, M. Asymmetric effects of diurnal warming on carbon allocation to leaves of marsh wetlands on the Tibetan Plateau. *Int. J. Digit. Earth* **2024**, *17*, 2419936. [CrossRef]
16. Wang, Y.; Shen, X.; Jiang, M.; Tong, S.; Lu, X. Daytime and nighttime temperatures exert different effects on vegetation net primary productivity of marshes in the western Songnen plain. *Ecol. Indic.* **2022**, *137*, 108789. [CrossRef]
17. Wen, Y.; Liu, X.; Yang, J.; Lin, K.; Du, G. NDVI indicated inter-seasonal non-uniform time-lag responses of terrestrial vegetation growth to daily maximum and minimum temperature. *Glob. Planet. Change* **2019**, *177*, 27–38. [CrossRef]
18. Liang, J.; Liu, X.; AghaKouchak, A.; Ciais, P.; Fu, B. Asymmetrical precipitation sensitivity to temperature across global dry and wet regions. *Earth's Future* **2023**, *11*, e2023EF003617. [CrossRef]
19. Li, T.; He, B.; Chen, D.; Chen, H.W.; Guo, L.; Yuan, W.; Fang, K.; Shi, F.; Liu, L.; Zheng, H.; et al. Increasing sensitivity of tree radial growth to precipitation. *Geophys. Res. Lett.* **2024**, *51*, e2024GL110003. [CrossRef]
20. Jia, Q.; Gao, X.; Jiang, Z.; Li, H.; Guo, J.; Lu, X.; Li, F.Y. Sensitivity of temperate vegetation to precipitation is higher in steppes than in deserts and forests. *Ecol. Indic.* **2024**, *166*, 112317. [CrossRef]
21. Wang, L.; Yue, Y.; Cui, J.; Liu, H.; Shi, L.; Liang, B.; Li, Q.; Wang, K. Precipitation sensitivity of vegetation growth in southern China depends on geological settings. *J. Hydrol.* **2024**, *643*, 131916. [CrossRef]
22. Lin, M.; Biswas, A.; Bennett, E.M. Spatio-temporal dynamics of groundwater storage changes in the Yellow River Basin. *J. Environ. Manag.* **2019**, *235*, 84–95. [CrossRef]
23. Ren, M.; Liu, Y.; Li, Q.; Song, H.; Cai, Q.; Sun, C. Responses of tree growth and intrinsic water use efficiency to environmental factors in Central and Northern China in the context of global warming. *Forests* **2022**, *13*, 1209. [CrossRef]
24. Song, M.; Jiang, X.; Lei, Y.; Zhao, Y.; Cai, W. Spatial and temporal variation characteristics of extreme hydrometeorological events in the Yellow River Basin and their effects on vegetation. *Nat. Hazard.* **2023**, *116*, 1863–1878. [CrossRef]
25. Zhang, S.; Gu, X.; Zhao, X.; Zhu, J.; Zhao, Y. Influences of climatic factors and human activities on Forest–Shrub–Grass suitability in the Yellow River Basin, China. *Forests* **2023**, *14*, 1198. [CrossRef]
26. Li, H.; Cao, Y.; Xiao, J.; Yuan, Z.; Hao, Z.; Bai, X.; Wu, Y.; Liu, Y. A daily gap-free normalized difference vegetation index dataset from 1981 to 2023 in China. *Sci. Data* **2024**, *11*, 527. [CrossRef] [PubMed]
27. Zhang, L.; Li, X.; Zheng, D.; Zhang, K.; Ma, Q.; Zhao, Y.; Ge, Y. Merging multiple satellite-based precipitation products and gauge observations using a novel double machine learning approach. *J. Hydrol.* **2021**, *594*, 125969. [CrossRef]
28. Nan, L.; Yang, M.; Wang, H.; Miao, P.; Ma, H.; Wang, H.; Zhang, X. Assessment of Spatio-Temporal Dynamic Vegetation Evolution and Its Driving Mechanism on the Kubuqi Desert Using Multi-Source Satellite Remote Sensing. *Remote Sens.* **2024**, *16*, 4769. [CrossRef]
29. Yan, Y.; Hong, S.; Chen, A.; Peñuelas, J.; Allen, C.D.; Hammond, W.M.; Munson, S.M.; Myneni, R.B.; Piao, S. Satellite-based evidence of recent decline in global forest recovery rate from tree mortality events. *Nat. Plants* **2025**, *11*, 731–742. [CrossRef] [PubMed]
30. Song, Y.; Gao, M.; Xu, Z.; Wang, J.; Bi, M. Temporal and spatial characteristics of soil salinization and its impact on cultivated land productivity in the BOHAI Rim region. *Water* **2023**, *15*, 2368. [CrossRef]
31. Wang, Y.; Kong, X.; Guo, K.; Zhao, C.; Zhao, J. Spatiotemporal change in vegetation cover in the Yellow River Basin between 2000 and 2022 and driving forces analysis. *Front. Ecol. Evol.* **2023**, *11*, 1261210. [CrossRef]
32. He, X.; Gao, M.; Wang, X.; Yang, Z.; Hu, Y. Assessment about wind erosion prevention effectiveness by ecological projects in the agro-pastoral zone of northern China. *J. Arid Environ.* **2025**, *231*, 105448. [CrossRef]
33. Li, H.; Xu, F.; Li, Z.; You, N.; Zhou, H.; Zhou, Y.; Chen, B.; Qin, Y.; Xiao, X.; Dong, J. Forest changes by precipitation zones in northern China after the Three-North Shelterbelt Forest Program in China. *Remote Sens.* **2021**, *13*, 543. [CrossRef]
34. Wei, S.; Li, X.; Wang, K.; Wang, T.; Piao, S. Two decades of persistent greening in China despite 2023 climate extremes. *Sci. China Earth Sci.* **2025**, *68*, 1064–1073. [CrossRef]
35. Yang, M.; Xue, L.; Liu, Y.; Liu, S.; Han, Q.; Yang, L.; Chi, Y. Asymmetric response of vegetation GPP to impervious surface expansion: Case studies in the Yellow and Yangtze River Basins. *Environ. Res.* **2024**, *243*, 117813. [CrossRef]
36. Shi, J.; Gao, Y.J.; Zou, Y.Y. Dynamic changes and driving factors of ecosystem service value (ESV) in the Northeast Forest Belt of China. *J. For. Res.* **2024**, *36*, 18. [CrossRef]
37. Chen, J.; Zhou, X.; Hruska, T.; Cao, J.; Zhang, B.; Liu, C.; Liu, M.; Shelton, S.; Guo, L.; Wei, Y.; et al. Asymmetric diurnal and monthly responses of ecosystem carbon fluxes to experimental warming. *Clean—Soil Air Water* **2017**, *45*, 1600557. [CrossRef]
38. Guo, J.; Liao, W.; Qimuge, H.; Xu, Y.; Wang, J. Seasonal analysis of spatial and temporal variations in NDVI and its driving factors in Inner Mongolia during the vegetation growing season (1999–2019). *Front. For. Glob. Change* **2025**, *8*, 1555385. [CrossRef]
39. Tan, J.; Piao, S.; Chen, A.; Zeng, Z.; Ciais, P.; Janssens, I.A.; Mao, J.; Myneni, R.B.; Peng, S.; Peñuelas, J.; et al. Seasonally different response of photosynthetic activity to daytime and night-time warming in the Northern Hemisphere. *Glob. Change Biol.* **2015**, *21*, 377–387. [CrossRef] [PubMed]
40. Xia, H.; Li, A.; Feng, G.; Li, Y.; Qin, Y.; Lei, G.; Cui, Y. The effects of asymmetric diurnal warming on vegetation growth of the Tibetan Plateau over the past three decades. *Sustainability* **2018**, *10*, 1103. [CrossRef]

41. Wan, S.; Xia, J.; Liu, W.; Niu, S. Photosynthetic overcompensation under nocturnal warming enhances grassland carbon sequestration. *Ecology* **2009**, *90*, 2700–2710. [CrossRef] [PubMed]
42. Shen, M.; Piao, S.; Chen, X.; An, S.; Fu, Y.; Wang, S.; Cong, N.; Janssens, I.A. Strong impacts of daily minimum temperature on the green-up date and summer greenness of the Tibetan Plateau. *Glob. Change Biol.* **2016**, *22*, 3057–3066. [CrossRef] [PubMed]
43. Piao, S.; Tan, J.; Chen, A.; Fu, Y.; Ciais, P.; Liu, Q.; Janssens, I.A.; Vicca, S.; Zeng, Z.; Jeong, S.J.; et al. Leaf onset in the northern hemisphere triggered by daytime temperature. *Nat. Commun.* **2015**, *6*, 6911. [CrossRef]
44. Li, W.; Zhang, Y.; Wang, N.; Liang, C.; Xie, B.; Qin, Z.; Yuan, Y.; Cao, J. Nocturnal water use partitioning and its environmental and stomatal control mechanism in *Caragana korshinskii* Kom in a semi-arid region of northern China. *Forests* **2023**, *14*, 2154. [CrossRef]
45. Zhao, L.; Chen, H.; Chen, B.; Wang, Y.; Sun, H. Drought shapes photosynthetic production traits and water use traits along with their relationships with leaves of typical desert shrubs in Qaidam. *Forests* **2022**, *13*, 1652. [CrossRef]
46. Nan, G.; Wang, J.; Han, L.; He, X.; Jiang, W.; Ma, J. Does slope cropland to natural and artificial conversion change patterns of soil moisture–carbon trade-offs in time and depth on the water-scarce Loess Plateau, China? *AGR Ecosyst. Environ.* **2025**, *385*, 109583. [CrossRef]
47. Zhou, M.; Wang, J.; Bai, W.; Zhang, Y.; Zhang, W. The response of root traits to precipitation change of herbaceous species in temperate steppes. *Funct. Ecol.* **2019**, *33*, 2030–2041. [CrossRef]
48. Xu, M.; Li, X.; Liu, M.; Shi, Y.; Zhou, H.; Zhang, B.; Yan, J. Spatial variation patterns of plant herbaceous community response to warming along latitudinal and altitudinal gradients in mountainous forests of the Loess Plateau, China. *Environ. Exp. Bot.* **2020**, *172*, 103983. [CrossRef]
49. White, A.B.; Kumar, P.; Tcheng, D. A data mining approach for understanding topographic control on climate-induced inter-annual vegetation variability over the United States. *Remote Sens. Environ.* **2005**, *98*, 1–20. [CrossRef]
50. Wei, B.; Peng, Y.; Lin, L.; Zhang, D.; Ma, L.; Jiang, L.; Li, Y.; He, T.; Wang, Z. Drivers of biochar-mediated improvement of soil water retention capacity based on soil texture: A meta-analysis. *Geoderma* **2023**, *437*, 116591. [CrossRef]
51. Yu, K.; Liu, J.; Zhang, X.; Li, P.; Li, Z.; Zhang, X.; Zhao, Y. Evapotranspiration fusion and attribution analysis in the upper and middle reaches of the Yellow River Basin. *J. Hydrol. Reg. Stud.* **2024**, *53*, 101773. [CrossRef]
52. Sun, S.; Bi, Z.; Mu, M.; Liu, Y.; Zhang, Y.; Li, J.; Liu, Y.; Zhou, Y.; Zhou, B.; Chen, H. Quantifying impacts of vegetation greenness change on drought over global vegetation zones. *Geophys. Res. Lett.* **2025**, *52*, e2024GL111634. [CrossRef]
53. Bai, Y.; Yu, P.; Wan, Y.; Wang, Y.; Liu, B.; Liu, Z. Promotion of tree transpiration by soil moisture replenishment along a larch hillslope in the Liupan Mountains, Northwest China. *J. Hydrol.* **2025**, *662*, 134041. [CrossRef]
54. Nehemy, M.F.; Mattos, C.R.C.; Oliveira, R.S.; Hirota, M.; Fan, Y.; Schlickmann, M.B.; Penha, D.; Giacomin, L.L.; Silva, J.S.G.M.; Rocha, M.; et al. Embolism resistance supports the contribution of dry-season precipitation to transpiration in eastern Amazon forests. *Proc. Natl. Acad. Sci. USA* **2025**, *122*, e2501585122. [CrossRef] [PubMed]
55. Wang, Y.; Wang, X.; Wang, Q. Temporal and spatial changes of vegetation phenology and their response to climate in the Yellow River Basin. *IEEE Access* **2023**, *11*, 141776–141788. [CrossRef]
56. Xiao, H.; Liu, Z.; Wan, J.; Chen, J.; Shi, Y. Experimental study of the soil water dissipation law of vegetated slopes under natural evaporation conditions. *Appl. Sci.* **2024**, *14*, 1105. [CrossRef]
57. Yang, K.; Guo, D.; Hua, W.; Pepin, N.; Yang, K.; Li, D. Tibetan Plateau temperature extreme changes and their elevation dependency from ground-based observations. *J. Geophys. Res. Atmos.* **2022**, *127*, e2021JD035734. [CrossRef]
58. Yang, C.; Tian, F.; Jin, H.; Fensholt, R.; Feng, L.; Tagesson, T. Assessing the elevational synchronization in vegetation phenology across Northern Hemisphere mountain ecosystems under global warming. *Glob. Planet. Change* **2025**, *252*, 104903. [CrossRef]
59. Zhao, C.; Wang, Y.; Qiu, Y.; Xie, Z.; Zhang, Y. Response of soil respiration to hydrothermal effects of gravel–sand mulch in arid regions of the Loess Plateau, China. *Soil Tillage Res.* **2023**, *231*, 105733. [CrossRef]
60. Kong, R.; Chu, Y.; Hu, Y.; Zhang, H.; Wang, Q.; Li, C. Diurnal Variation Reveals the Characteristics and Influencing Factors of Cool Island Effects in Urban Blue-Green Spaces. *Forests* **2024**, *15*, 2115. [CrossRef]
61. Bao, Z.; Zhang, J.; Wang, G.; Guan, T.; Jin, J.; Liu, Y.; Li, M.; Ma, T. The sensitivity of vegetation cover to climate change in multiple climatic zones using machine learning algorithms. *Ecol. Indic.* **2021**, *124*, 107443. [CrossRef]
62. Lan, X.; Li, R.; Wang, X.; Zhou, T.; Li, Y.; Duo, J.; Sun, J. Vegetation dynamics and sensitivity responds to climate change in the upstream of Yellow River, China. *Ecosyst. Health Sustain.* **2025**, *11*, 0292. [CrossRef]
63. Guo, B.; Liu, Y.; Fan, J.; Lu, M.; Zang, W.; Liu, C.; Wang, B.; Huang, X.; Lai, J.; Wu, H. The salinization process and its response to the combined processes of climate change–human activity in the Yellow River Delta between 1984 and 2022. *Catena* **2023**, *231*, 107301. [CrossRef]
64. Singh, A. Soil salinization management for sustainable development: A review. *J. Environ. Manag.* **2021**, *277*, 111383. [CrossRef]
65. Marra, F.; Armon, M.; Morin, E. Coastal and orographic effects on extreme precipitation revealed by weather radar observations. *Hydrol. Earth Syst. Sci.* **2022**, *26*, 1439–1458. [CrossRef]

66. Dallan, E.; Marra, F.; Fosser, G.; Marani, M.; Formetta, G.; Schar, C.; Borga, M. How well does a convection-permitting regional climate model represent the reverse orographic effect of extreme hourly precipitation? *Hydrol. Earth Syst. Sci.* **2023**, *27*, 1133–1149. [CrossRef]
67. National Standardization Administration; State Administration for Market Regulation. *Soil Mapping—Specifications for the Symbols, Colors and Legends of Soil Texture, pH and Salinization Maps at the Scale of 1:25,000~1:500,000*; State Administration for Market Regulation: Beijing, China, 2025.
68. Zhang, X.; Li, Y.; Li, F. Spatial distribution characteristics of soil water–salt gradients in the ecological buffer zone of arid zone lakes and their influencing factors. *J. Clean. Prod.* **2024**, *444*, 141299. [CrossRef]
69. Wu, H.; Yu, M.; Sun, Y.; Tan, G.; Ji, Z. Prediction of net primary productivity in the middle-to-high latitudes of Eurasia based on snow and soil temperature. *Atmos. Ocean. Sci. Lett.* **2024**, *18*, 100535. [CrossRef]
70. Dong, G.; Fan, L.; Fensholt, R.; Frappart, F.; Ciais, P.; Xiao, X.; Sitch, S.; Xing, Z.; Yu, L.; Zhou, Z.; et al. Asymmetric response of primary productivity to precipitation anomalies in Southwest China. *Agric. For. Meteorol.* **2023**, *331*, 109350. [CrossRef]
71. Jin, X.; Lu, S.; Ji, Y.; Qin, Y.; He, G. Assessing the Ecosystem Service Value of Small-Scale Landscapes in Rural Tourism Destinations in the Yangtze River Delta. *Sustainability* **2025**, *17*, 9410. [CrossRef]
72. Liu, C.; Liu, J.; Zhang, L.; Shrestha, U.B.; Luo, D.; Wei, Y.; Wang, J. Assessing Climate and Land Use Change Impacts on Ecosystem Services in the Upper Minjiang River Basin. *Remote Sens.* **2025**, *17*, 1884. [CrossRef]

Disclaimer/Publisher's Note: The statements, opinions and data contained in all publications are solely those of the individual author(s) and contributor(s) and not of MDPI and/or the editor(s). MDPI and/or the editor(s) disclaim responsibility for any injury to people or property resulting from any ideas, methods, instructions or products referred to in the content.